# Dynamic damage identification using linear and nonlinear testing methods on a two-span prestressed concrete bridge

J. Mahowald, S. Maas, F. Scherbaum, & D. Waldmann
*University of Luxembourg, Faculty of Sciences, Technology and Communication, Luxembourg, Luxembourg*

A. Zuerbes
*Fachhochschule Bingen, Bingen, Germany*

ABSTRACT: In this paper dynamic testing methods on a two span prestressed concrete bridge are examined to evaluate the ability on damage assessment on civil engineering structures in situ. The testing methods are based on analysing modal parameters, i.e. the eigenfrequencies and the modeshapes, as well as the calculation of the corresponding flexibility matrix. Variations on them are shown for different damage states, realised by continuously cutting tendons and loading the bridge with an experimental mass of 245t. Moreover, the evaluation of nonlinear parameters as the amplitude dependency of the eigenfrequencies is also presented. For the different damage states cracks are noticed at the different cutting sections. As nonlinear parameter and the modeshapes do not retrieve clear indications on the damage, the changes of the eigenfrequencies and the flexibility matrices demonstrate, in contrast, clearly the capability on damage assessment on the investigated object.

## 1 INTRODUCTION

Today, the reliability of civil engineering structures, especially bridges is a crucial issue regarding the growing amount due to expanding mobility facilities. Nowadays, as the cost for planning and construction are continuously increasing, service guarantees and regular inspections get more and more important to assure the serviceability of the engineering structures. Furthermore, these inspections encounter difficulties due to the sometimes complex handing, associated with huge costs. Therefore, research is conducted on several kinds of inspection techniques to simplify and improve existing testing procedures and to introduce new methods. Also the University of Luxembourg studies on this topic, examining condition control of civil engineering structures using dynamic and static testing methods. Dynamic and static tests have the advantage that they can easily be set up or implemented for condition monitoring, but are not always easy to interpret, as they are influenced by environmental impacts (Peeters et al. 2001). Nevertheless, laboratory results demonstrate the possible use of the introduced testing methods, as they show the changes of the stiffness of a structure by the retrieved investigated parameters (Mahowald et al. 2010).

In this paper the dynamic evaluation of an in situ object is presented. The explored two-span prestressed box girder bridge is continuously damaged artificially in order to demonstrate the reliability of dynamic and static testing methods. The possibility to conduct these tests is unique; as the bridge is demolished afterwards, reason of changed urban planning.

### 1.1 *Description of the bridge*

The investigated bridge (Fig. 1), which is called Champangshiel, was built from 1965 to 1966 and connects the centre of Luxembourg with the district Kirchberg. It is a two span prestressed concrete bridge with different span length (Fig. 2). The length of the bridge is 102 m, divided into two fields of 65 m and 37 m in length. The superstructure of the bridge is a prestressed box girder with 32 parabolic, 24 upper straight lined and 20 lower straight lined subsequently injected tendons (Figs 3-4). The roadbed has a width of 12.5 m and the box girder of 6.5 m with a height of 2.62 m, as illustrated on Figure 3. The bridge is made of concrete B450 and the tendons of Steel ASTM A.416 57T. The superstructure is supported by two abutments and one column made of reinforced concrete. At the west abutment (abutment of the large field) is a mobile bearing made of a steel roll, whereas on the east abutment, the bearing is fixed. Between the superstructure and the substructure over the pylon an elastomeric support is placed. In 1987, 56 external prestressed steel cables were added into the box girder of the large field due to additional safety (Figs 3-4) (Scherbaum et al. 2011).

Figure 1. Picture of the bridge in winter 2010.

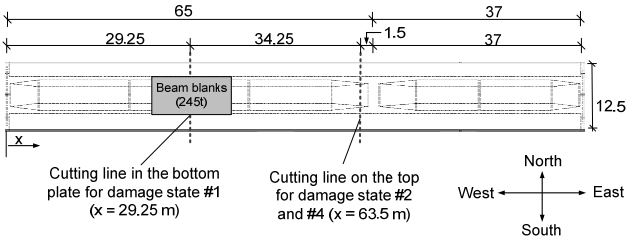


Figure 2. Longitudinal Section of the bridge with the cutting sections and the position of the experimental mass.

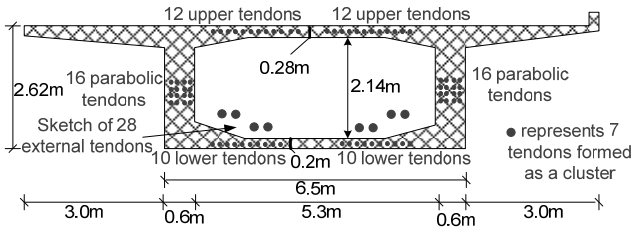


Figure 3. Schematic cross section of the bridge with all the tendons.

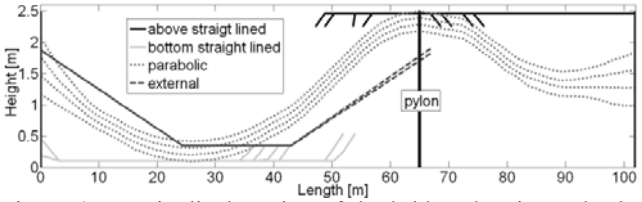


Figure 4. Longitudinal section of the bridge showing only the tendons.

## 2 TESTING PROCEDURES

### 2.1 *Damage scenarios*

In order to validate the presented testing methods for damage assessment, tests are conducted for different damage scenarios. Table 1 summarises the different damage states (intact #0 to the most damaged #4) by continuously cutting a defined number of tendons at two different sections of the bridge, as illustrated on Figure 2.

Figures 5a-5d illustrates schematically the different damage scenarios for the selected sections. These damage states are crucial to evaluate the sensitivity of the test results according the severity of introduced damage and formation of cracks. This is achieved by firstly cutting a defined number of tendons and secondly by loading the bridge with an additional experimental mass of 245 t, consisting of 38 beam blanks from ArcelorMittal (Fig. 6). One has to add, that for each damage state, except for #4, the bridge is loaded with the experimental mass for static and additional dynamic measurements (data not shown).

Table 1. Description of the damage scenarios according to the cutting sections shown on Figure 2.

| Damage state | Cutting tendons | Percentage cutting (100% equals all tendons in the defined section) | |
|---|---|---|---|
| | | x=29.25 m | x=63.5 m |
| # 0 | Undamaged state | 0% | 0% |
| # 1 | 20 straight lined tendons in the lower part of the bridge (x=29.25 m), (Fig. 5a) | 33.7% | 0% |
| # 2 | 8 straight lined tendons in the upper part of the bridge over the pylon (x=63.5 m), (Fig. 5b) | 33.7% | 12.6% |
| # 3 | 56 external tendons, (Fig. 5c) | 46.1% | 24.2% |
| # 4 | 16 straight lined and 8 parabolic tendons in the upper part of the bridge (x=63.5 m), (Fig. 5d) | 46.1% | 62.12% |

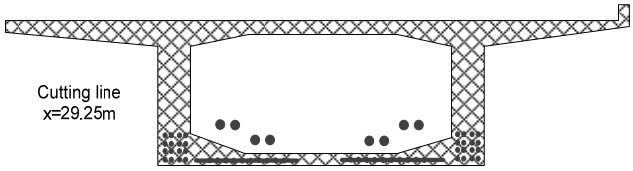


Figure 5a. Damage state #1 for the cutting line at x=29.25 m.

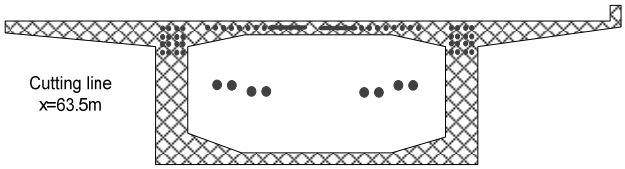


Figure 5b. Damage state #2 for the cutting line at x=63.5 m.

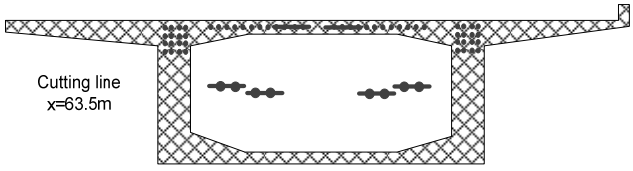


Figure 5c. Damage state #3 for the cutting line at x=63.5 m.

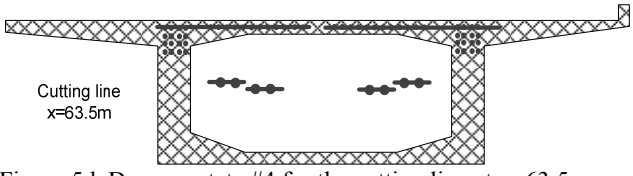


Figure 5d. Damage state #4 for the cutting line at x=63.5 m.

Figure 6. Experimental mass, after loading with 31 of 38 beam blanks.

## 2.2 *Crack formation*

Due to the cutting tendons and loading with an experimental mass of 245 t, cracks are formed for the different damage scenarios. Table 2 summarises the appearance of the different cracks, essential for the validation of the presented test results.

Table 2. Description of the appearance of cracks according the damage states and loading.

| *Description* | *Cracks* |
|---|---|
| #1 | Shear cracks due to the new anchorage points of the prestressed cables by cutting the lower 20 straight lined prestressed cables (black cracks, dashed line on Figure 7) |
| #1-loaded | #1 + one crack in the girder at the north side up to 1.5m from the bottom line (dark grey cracks, solid line on Figure 7) and 1m on the south side at the cutting line of the lower 20 straight lined tendons |
| #3 | #1-L + growing of the existing cracks and formation of new cracks at 0.45L (grey cracks, dashed line on Figure 7) + small crack between the holes on the upper side with loading (Fig. 8). |
| #4 | #3 + crack above the pylon (grey cracks, solid line on Figure 7 and Figure 8) |

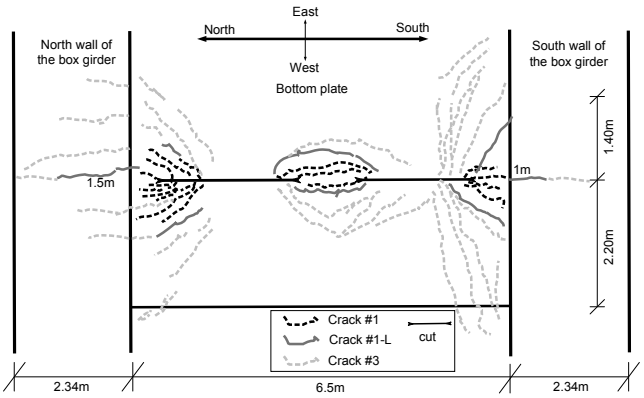


Figure 7. Schematic view of the crack appearance at the bottom plate for the cutting line at x=29.25 m.

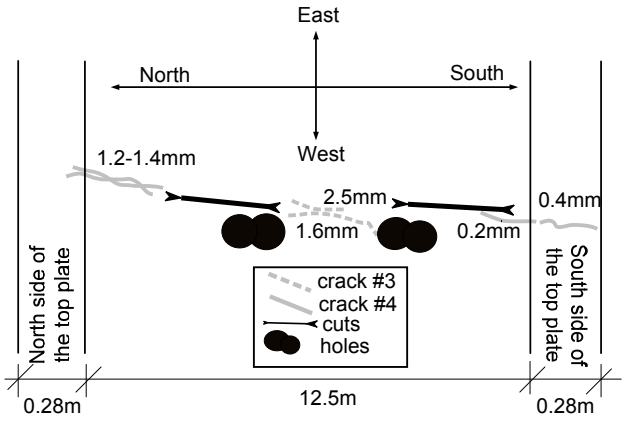


Figure 8. Schematic view of the crack appearance at the top plate for the cutting line at x=63.5 m.

## 2.3 *Dynamic measurements*

For the dynamic tests three different test procedures with two different exciters are achieved for each damage scenario. The use of two exciters allows having a waste force and frequency excitation spectrum from 500 N to 10000 N and from 1 Hz to 20 Hz. This is used for the analysis on the excitation force amplitude dependency of the eigenfrequencies, which is a non-linear phenomenon. For this, different force amplitudes are applied on the bridge: 0.5 kN, 1.25 kN and 2.5 kN for the electromagnetic shaker, type TIRA and 1.25 kN, 2.5 kN, 5 kN and 10kN for the unbalanced mass exciter, called Netter vibration system (data with 5 kN and 10 kN excitement for the Netter excitation system is not shown). The applied force excitations are swept sine functions with a sweep rate of 0.02 Hz/s. For the electromagnetic shaker for an excitation force of 0.5 kN, the swept sine runs from 1.25 to 20Hz, for 1.25kN from 2 to 20Hz and for 2.5kN from 3 to 20Hz, due to the limits of the electromagnetic shakers for high excitation forces. For the Netter vibration system different physical limits exist; here the swept sine runs for an excitation force of 1.25 kN from 1 to 5 Hz, for 2.5 kN from 1 to 20Hz, for 5 kN from 2.5 to 20 Hz and for 10 kN from 4 to 20Hz. Moreover, an impact test is done using a 12 lb modal hammer of type Dytran 5803A ICP for evaluating statistical analysis by the University of Liège (Nguyen et al. 2012). The 22 accelerometers of type PCB 393B04 are put on both sides of the bridge in a coarse grid, as shown on Figure 9 in black. The sample rate for the force transducers of type HBM U10M and accelerometers is 1000Hz. The electromagnetic shaker and the Netter vibration system is put on the bridge as illustrated on Figure 9. For the dense measurement grid, the bridge is excited only by the electromagnetic shaker with a force of 0.5 kN due to time limits and to have the widest range of the frequency spectrum. For this grid, measurements are conducted

by placing the transducers on each position in white and black on Figure 9. They are shifted five times of about 2 m (5*20=100 positions) to capture the movements at all presented positions, needed to obtain proper values to calculate the modeshapes. For evaluating and visualisation of these, each transducer position is numbered, beginning in the west with 1 to 50 in the east. In this paper, exclusively the Northern line is discussed.

Furthermore, only one dynamic measurement series per day is achieved due to time reasons, repeated for each damage scenario presented on Table 1.

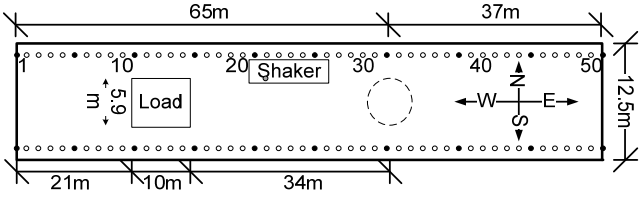


Figure 9. Experimental setup for the dynamic testing methods: Black circles: the position of the accelerometers for the coarse measurement grid. White circles: the additional positions for the dense measurement grid.

For the evaluation of modal parameters, Mescope Software is used operating the Global Polynomial Method to yield the presented modal results.

## 3 TEST RESULTS

Below the test results for the different measurement series are presented with first the eigenfrequencies, followed by the evaluation of the modeshapes as well as the corresponding calculations of the flexibility matrices and their changes for the different damage states. For this, one has to add that only the predominant modes are presented, shown on Figure 10, illustrating the frequency response functions for the intact state. These eigenfrequencies are also found for all other damage states and are named henceforth B1, T2, B3, B4, T4, T5 and T6, where B stands for bending and T for torsional modes.

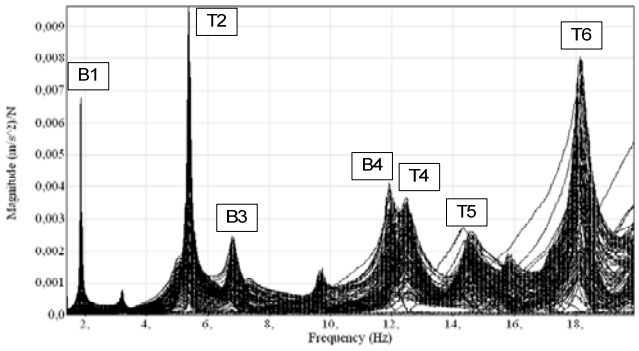


Figure 10. Frequency response functions of the intact state for the dense measurement grid.

### 3.1 *Eigenfrequencies*

As examples of the changes of the eigenfrequencies only the first bending mode, named B1, the second torsional mode (T2) and the fourth bending mode (B4) are presented in the following. Regarding the first eigenfrequency on Figure 11, one recognises a drastic decrease according the damage states. Here for damage state #1 a diminishing of 3% is identified compared to the intact state #0. The reason is the appearance of a first crack in the bottom plate of the bridge yielding a loss in stiffness. Further, when cutting 8 of the above tendons, i.e. 12.6% of the tendons in the top plate for this damage state #2 (Fig. 5b), no crucial additional cracks are observed. Afterwards, for damage state #3 and #4, when cutting the external and 40% of the above tendons (Figs 5c, d) existing crack expand and more cracks occurred (Fig. 7), marked by a decrease of the eigenfrequency by 10% and up to 18% for damage state #3 and #4 respectively, presented on Figure 12.

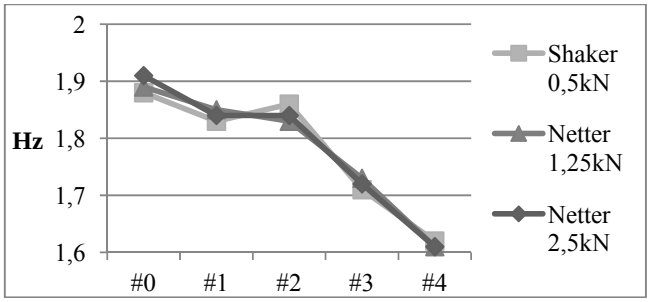


Figure 11. First eigenfrequencies (B1) for the different damage states and different excitation force amplitudes.

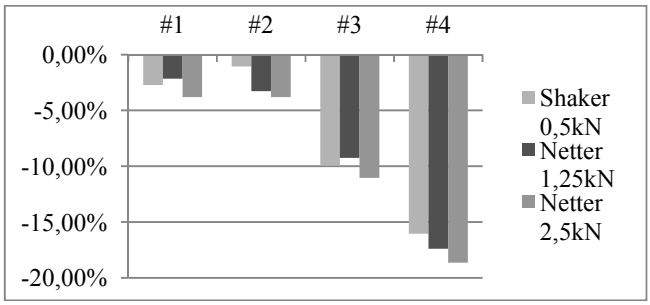


Figure 12. Percentage decrease of the first eigenfrequencies (B1) for the different damage states and excitation force amplitudes compared to the intact state #0.

In contrast, the changes of the eigenfrequencies of the second torsional mode T2 do not correlate with the damage, illustrated on Figures 13-14. Here no information according the severity on the damage can be made and the increase in scenario #2 is not understood.

On the contrary, the eigenfrequencies of the fourth bending mode (B4) on Figure 15 show also a significantly decrease due to damage. Here, for the evaluation of the percentage decrease on Figure 16 from damage state #1 to the intact state #0, variations up to 2% are recognised, increased to 6% for damage state #3 and to 8% for damage state #4.

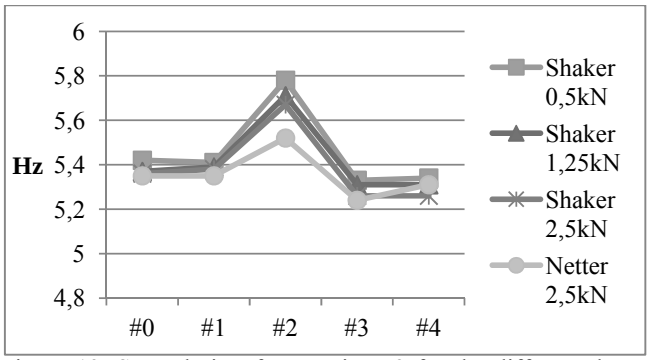

Figure 13. Second eigenfrequencies T2 for the different damage states and excitation force amplitudes.

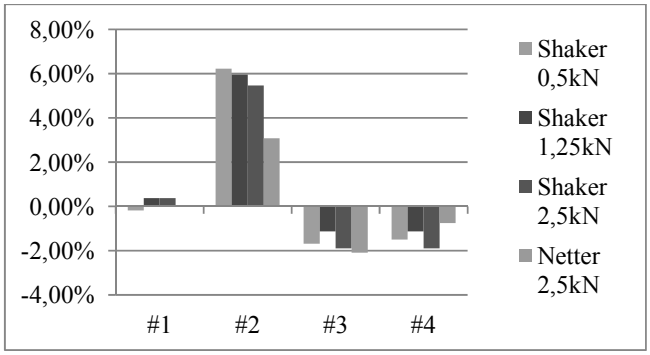

Figure 14. Percentage decrease of the second eigenfrequencies (T2) for the different damage states and excitation force amplitudes compared to the intact state #0.

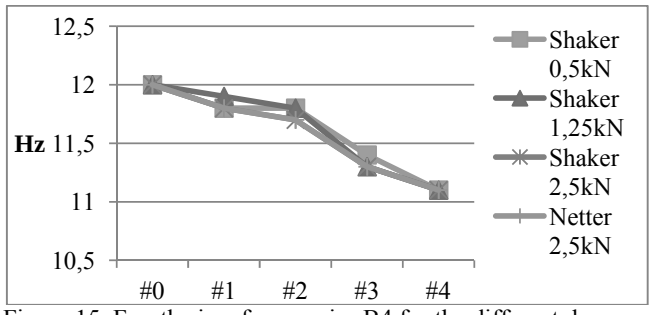

Figure 15. Fourth eigenfrequencies B4 for the different damage states and excitation force amplitudes.

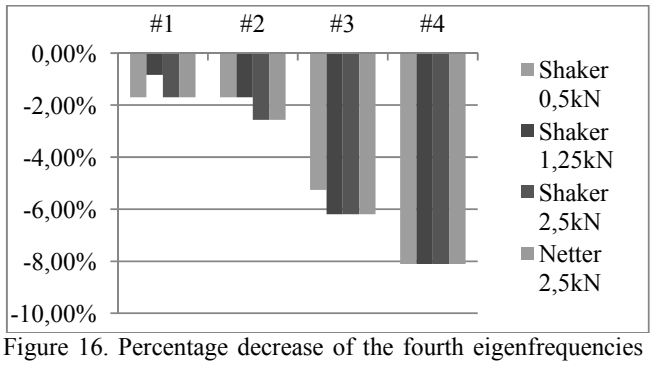

Figure 16. Percentage decrease of the fourth eigenfrequencies (B4) for the different damage states and excitation force amplitudes compared to the intact state #0.

One can say that for these examples of the eigenfrequencies and crack formation, damage identification is possible regarding the bending modes B1 and B4, as they show clear variations according the damage in the bridge, and, therefore, reliable for damage identification. Nevertheless, regarding the second torsional mode T2, no significant information can be retrieved, making damage assessment using only the eigenfrequencies ambitious.

### 3.2 *Amplitude dependency of the eigenfrequencies*

Now, regarding the excitation force amplitude dependency of the eigenfrequencies for the presented examples, no pattern according the severity of the damage can be recognised, shown on Figure 17. For the first eigenfrequency B1, the amplitude dependency is around -1.5% for the intact state, meaning from an excitation force of 2.5 kN for the Netter excitement to 0.5 kN for the shaker excitement, increased to 1% for damage state #2 and varying from -0.5% to 0.5% for damage state #3 and #4. Neither for the second torsional mode T2 and fourth bending mode B4 an accurate pattern is noticed, making the amplitude dependency in this case not reliable for indications on damage.

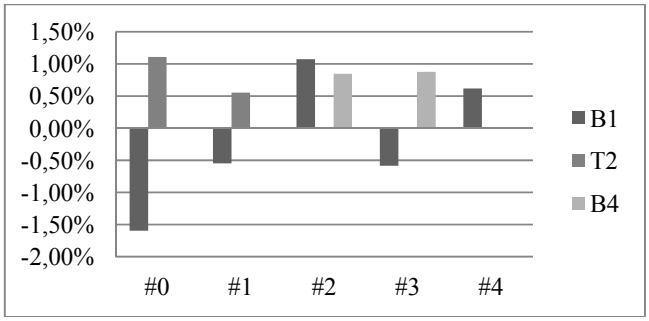

Figure 17. Excitation force amplitude dependency of the first eigenfrequency for Netter excitement of 2.5 kN to 0.5 kN from the shaker excitement.

### 3.3 *Modeshapes*

The modeshapes of all the evaluated eigenmodes shown on Figure 10 are presented in this section. They are, as already introduced in the experimental part, captured by a dense measurement grid, spaced at 2 m apart from each transducer position (Fig. 9). In order to compare each modeshapes from all the damage states to the intact states, each mode is normalised to Unit Modal Mass (UMM). On Figure 18 the modeshape for the first eigenmode B1 is displayed. For this it is difficult to retrieve any information out of the presented curves. The changes due to damage are very small and hard to identify.

In contrast, looking at the second torsional mode T2 on Figure 19, big variations can be recognised, but cannot be associated to damage, as the amplitudes are either higher or lower the curve for the intact state. In addition, for the third bending mode B3 on Figure 20, the same behaviour is revealed. Neither here, especially between transducer positions 20 to 45, is a logical order of the curves recognised,

concluding that no unique pattern can be identified for these two modes.

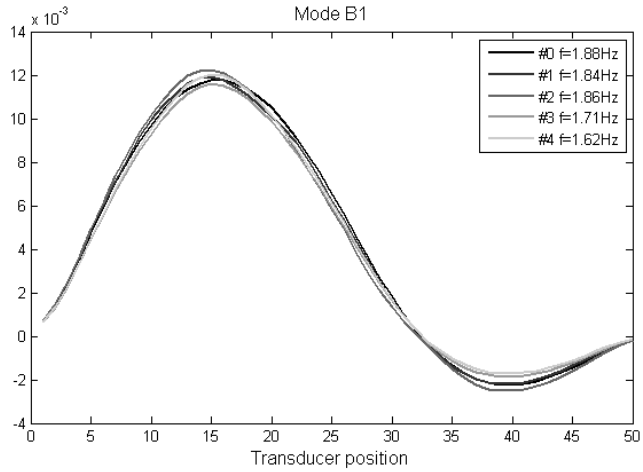


Figure 18. UMM-normalised modeshape of the first bending mode (B1) for the unloaded bridge.

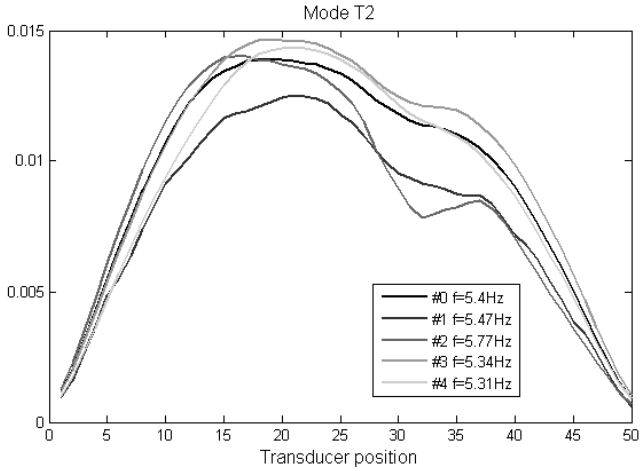


Figure 19. UMM-normalised modeshape of the second torsional (T2) mode for the unloaded bridge.

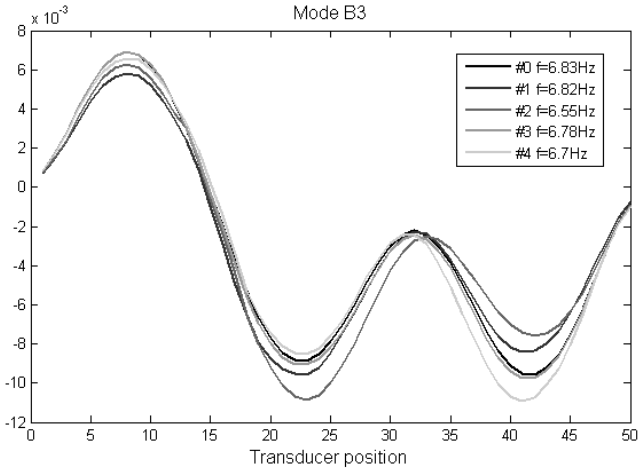


Figure 20. UMM-normalised modeshape of the third bending mode (B3) for the unloaded bridge.

However, for the fourth bending mode B4 on Figure 21, the fourth torsional mode T4 on Figure 22 and the fifth torsional mode T5 on Figure 23 variations to the intact state are clearly identifiable. Here, around transducer position 7 to 15 for B4 for example, differences according the increased damage are noticed. As well for the fourth torsional mode T4 the same behaviour can be discovered. For the fifth torsional mode T5, the changes are even more exposed; concluding that damage identification for these modes is possible.

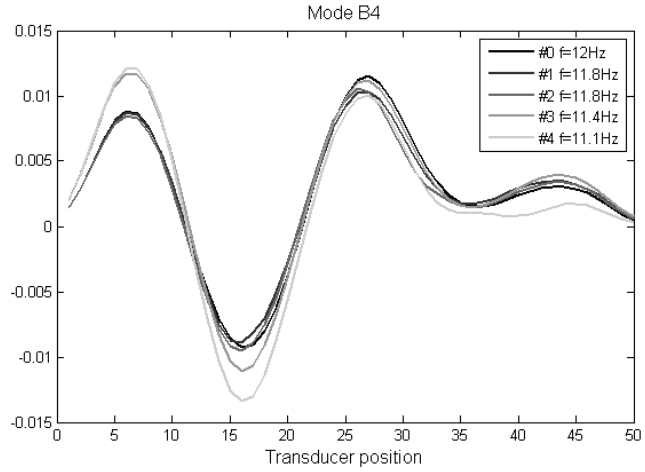


Figure 21. UMM-normalised modeshape of the fourth bending (B4) mode for the unloaded bridge.

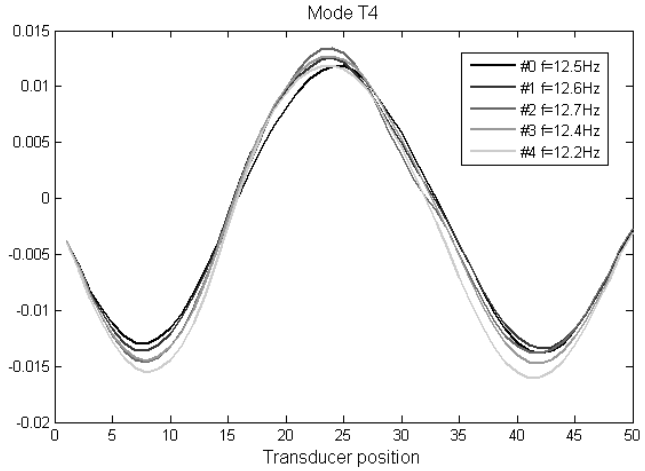


Figure 22. UMM-normalised modeshape of the fourth torsional mode (T4) for the unloaded bridge.

Finally, for the sixth torsional mode (T6), as for the first bending mode B1, no considerable changes due to damage are recognised. The mode seems not be as much affected by the changed stiffness as the other ones.

Concluding, one can state that some modes, for example the fourth bending mode B4, as already observed for the eigenfrequencies are more affected by a changed structure than other modes, like the second torsional modes T2, making damage identification possible but difficult. However, even regarding the modes on which damage identification seems possible, the issue on the localisation of damage remains unsolved.

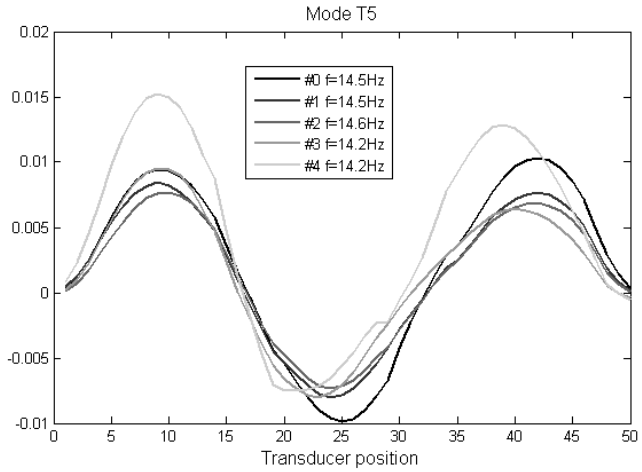


Figure 23. UMM-normalised modeshape of the fifth torsional mode (T5) for the unloaded bridge.

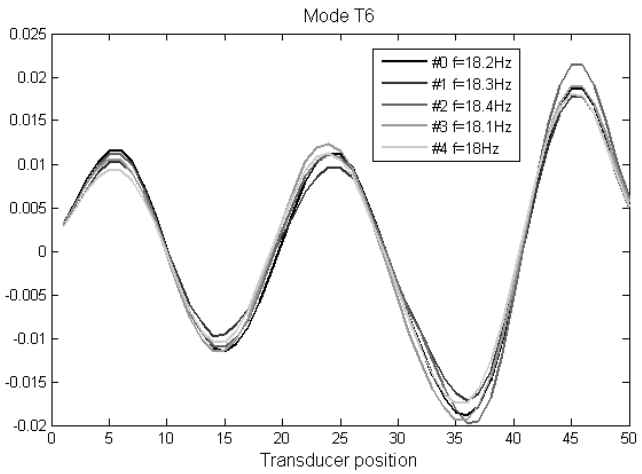


Figure 24. UMM-normalised modeshape of the sixth torsional mode (T6) for the unloaded bridge.

### 3.4 *Flexibility matrix*

Since a set of modal parameters is yield out of the measurement data, i.e. normalised modeshapes and eigenfrequencies, the flexibility matrix can be calculated with the revealed parameters for each damage state. This matrix represents the inverse stiffness matrix and is, therefore, an indication of the loss of the stiffness due to cracks. It is calculated according Equation 1, retrieved out of the UMM-normalised modeshapes Φ and the angular eigenfrequencies ω=2πf, where k defines the mode and N the total number of modes considered in the calculation of the flexibility matrix. Further, as already emphasised in the previous sections, also here for the calculation of the flexibility matrix the 7 predominant modes are utilised (N=7):

$$[K]^{-1} = \sum_{k=1}^{N} \{\Phi_k\} \cdot \frac{1}{\omega_k^2} \{\Phi_k\}^T = [F] \qquad (1)$$

Figures 25-26 illustrate the diagonal elements of the flexibility matrices for the intact state #0 and damage state #4 in the modal decomposition mode, meaning that the flexibility matrix is calculated considering only one mode (solid lines). For better visualisation, the sum of all the 7 modes is presented also on the graphs (dashed line). Here, one can recognise that the flexibility matrix is determined already by the first two modes, i.e. the first bending mode B1 and the second torsional mode T2. This is due to the fact that according Equation 1 the UMM-modeshapes are divided by the square of the angular frequencies, which increase considerably for higher modes (from 1.8Hz to 18Hz) and, therefore, the impact of the higher modes diminishes in the calculation of the flexibility matrix.

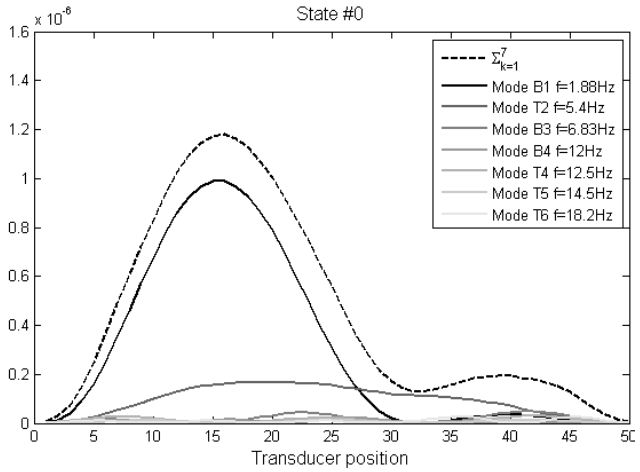


Figure 25. Modal decomposition of each of the seven modes and of their sum of the diagonal elements of the flexibility matrix for the intact state.

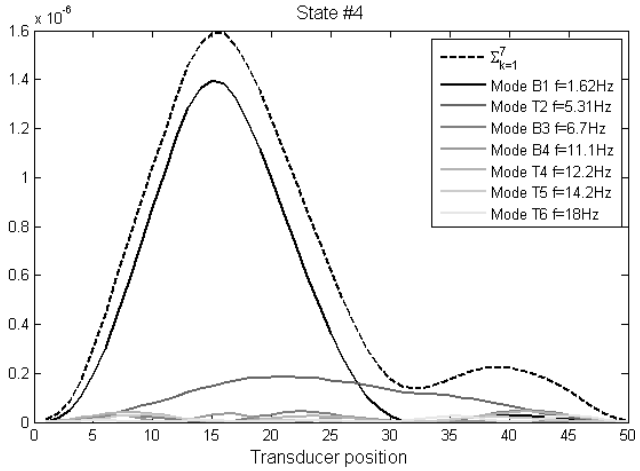


Figure 26. Modal decomposition of each of the seven modes and of their sum of the diagonal elements of the flexibility matrix for damage state #4.

To compare the different damage states the flexibility matrices (only the sum for all 7 modes) of all the scenarios are presented on Figure 27. Variations according the damage can clearly be seen. Here around transducer position 15, where the highest damage occurred (cracks on Figure 7) the biggest changes are noticed. Damage state #4 shows the highest value concluding to the biggest loss in stiff-

ness, followed by damage state #3 and so forth. Hence, here the right order according the different damage states is identified and, moreover, localisation of damage becomes feasible.

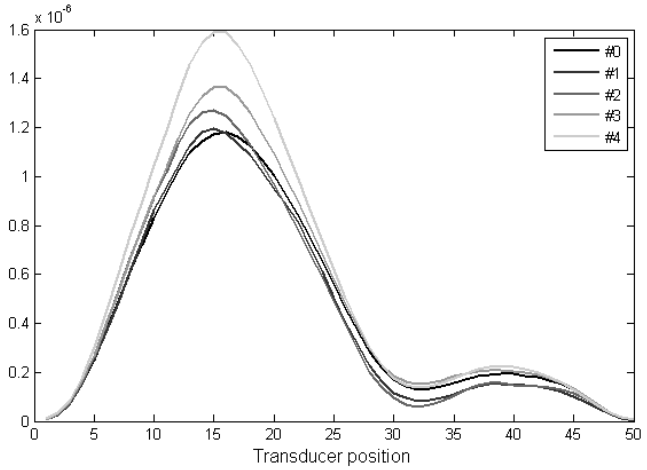


Figure 27. Diagonal elements of the flexibility matrices for the unloaded bridge.

### 3.5 *Flexibility difference*

Furthermore, for a better visualisation of the variations of the flexibility matrices, the following Figure 28 shows the differences of the diagonal elements of the flexibility matrices according Equation 2, in which $d_{\#i}$ marks the diagonal elements in each flexibility matrix for the i-th damage state:

$$\delta = |d_{\#i} - d_{\#0}| \quad (2)$$

This is a similar technique used in literature (Pandey et al. 1995, Lenzen 2009) for better localisation of damage and presenting the changes of the flexibility matrices. Also here, one can see clear variations from one damage scenario to the other, as already observed on Figure 27. With increasing damage, compared to the intact state, the changes get evident, making the evaluation of the flexibility matrices a trustful indicator on the loss of stiffness, i.e. the formation of cracks.

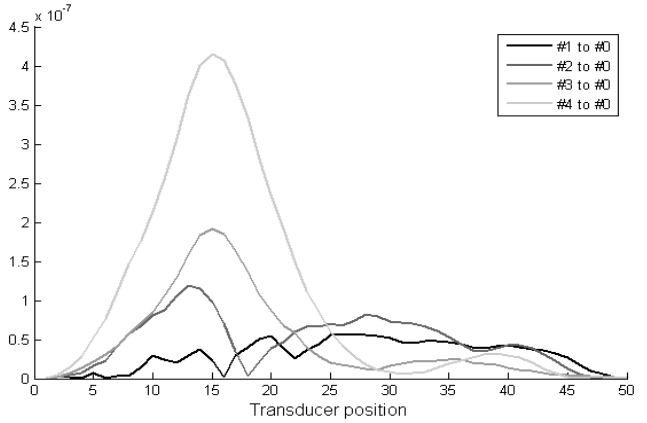


Figure 28. Difference of the diagonal elements δ of the flexibility matrices for all damage states compared to the intact state #0.

## 4 CONCLUSION

The investigation of the dynamic tests reveals a large amount of information on the different examined parameters. Here nonlinear, i.e. the excitation force amplitude dependency, as well as linear parameters, i.e. the evaluation of the eigenfrequencies and the modeshapes, are analysed. Regarding nonlinear parameters, no exact statement on the condition can be made, since the amplitude dependency does not show any correlation to the damage.

In contrast, for the linear values, the most influenced parameters are the eigenfrequencies and modeshapes for specific eigenmodes. Regarding the eigenfrequencies, clear decreases are recognisable and are conform to the damage introduced into the bridge. These variations on the eigenfrequencies identify the changes on the structure, but do not afford localisation considering only this parameter. Therefore, the analysis of the modeshapes is evaluated for this issue. However, the variations of these do not retrieve any trustful results on the location of damage. Changes are evident, but the localisation regarding the identified modes is difficult. Thus, the flexibility matrices, calculated from the identified modal parameters, are analysed to discover the loss in stiffness. They yield accurate results indicating and even, in contrast to the eigenfrequencies and modeshapes, localising damage in the bridge. Moreover, the differences of the diagonal elements of the flexibility matrices show significantly the location of damage, concluding that this investigated parameter is evident according damage and therefore adequate for further research on damage assessment on civil engineering structures in situ.

## REFERENCES


Lenzen, A. 2009, Markov-Parameter als Schädigungsindikator bei der Systemidentifikation in der Baudynamik, *VDI-Berichte 2063, 3.VDI-Fachtagung: Baudynamik*, Kassel 14-15.Mai 2009, 109-120.

Mahowald, J., Bungard, V., Maas, S., Waldmann, D., Zuerbes, A. & De Roeck, G. 2010, Comparison of linear and nonlinear static and dynamic behaviour of prestressed and non-prestressed concrete slab elements, *Proceedings ISMA 2010*, Leuven, 717-728.

Nguyen, V. H., Rutten, C., Golinval, J.-C., Mahowald, J., Maas, S., Waldmann, D. 2012, Damage Detection on the Champangshiehl Bridge using Blind Source Separation, *IALLCE 2012, Third International Symposium on Life-Cycle Civil Engineering*, Vienna October 3-6 2012.

Pandey, A.k. & Biswas, M. 1995, Experimental Verification of Flexibility Difference Method for locatin damage in structures, *Journal of Sound and Vibration,* Vol. 184 (2), 311-328.

Peeters, B & De Roeck, G. 2001, One-year monitoring of the Z24-Bridge: environmental effects versus damage events, *Earthqueke Engineering and Structural Dynamics*, Vol. 30, 149-171.

Scherbaum, F. & Mahowald, J. 2011, Report Bridge Champangshiehl 2, University of Luxembourg, unpublished